

# Decoupler Design for MIMO Antennas of USB Dongle Applications Using Ground Mode Coupling Analysis

Zeeshan Zahid<sup>1, \*</sup>, Longyue Qu<sup>2</sup>, Hyung Hoon Kim<sup>3</sup>, and Hyeongdong Kim<sup>2</sup>

**Abstract**—In this paper, the impact of decoupler type has been analyzed on the performance of planar inverted-F antenna (PIFA)-based multiple-input multiple-output (MIMO) antenna. A T-type and a loop-type decoupler have been employed for the isolation of the MIMO antennas, and the performances of the two cases have been compared. The decouplers have been selected based on their different coupling mechanisms with the dominant ground mode. The antennas have been designed for the ground configuration of a USB dongle operating at 2.45 GHz band. Characteristic mode analysis of the ground plane has been carried out, and the MIMO systems have been analysed based on the coupling among the antenna, decoupler and the dominant characteristic mode of the ground plane. It has been observed that the coupling between the decoupler and the ground mode significantly affects the radiation efficiency as well as the diversity performance of the MIMO antenna.

## 1. INTRODUCTION

The importance of electrically small antennas has been emphasized by recent advancements in mobile device technology. The demand for high data throughput has emphasized the importance of multiple-input multiple-output (MIMO) antennas for mobile devices [1, 2]. High diversity performance and good radiation efficiency are desirable features of modern MIMO antennas. Planar inverted-F antennas (PIFAs) have been widely utilized in mobile devices due to their advantages of compact size, low cost and easy fabrication [3, 4]. Various non MIMO single band [5, 6] and multiband antennas [7, 8] have been proposed for USB dongle applications whereas MIMO antennas for USB dongles operating at WLAN band are proposed in [9–11]. The diversity performance of MIMO antennas depends on the employed decoupler; therefore, several decoupling configurations have been proposed in the literature. The impact of parasitic monopoles on dual-slot-element antennas for mobile terminals was analyzed in [12]. The studies reported in [13–17] discussed a protruded T-shaped stub for high isolation and good diversity performance. A floating parasitic inter-digit decoupler was proposed for ultra-wideband isolation [18]. Different configurations of slits [19–21] and slot-type decouplers [22] were employed to provide good isolation. A tunable ground coupled loop-type isolator ensured high isolation between ground radiation MIMO antennas [23]. Metal rim of mobile device was utilized to control the orthogonal characteristic modes of the ground plane for MIMO operation in [24]. In [25], the authors applied characteristic mode theory to generate harmonized orthogonal radiation modes for MIMO operation. Characteristic modes can also be utilized to design pattern reconfigurable MIMO antennas for mobile devices [26, 27]. Various pattern reconfigurable MIMO antennas have also been proposed such as using U-slot [28], switches [29, 30], parasitic radiators [31] and partial stepped ground plane [32]. Concentric slot based loop based MIMO array was proposed in [33] for 4G/5G mobile applications.

---

*Received 26 September 2018, Accepted 18 November 2018, Scheduled 28 November 2018*

\* Corresponding author: Muhammad Zeeshan Zahid (zeeshanzahid@mcs.edu.pk).

<sup>1</sup> Department of Electrical Engineering, College of Signals, National University of Sciences and Technology, Rawalpindi, Pakistan.

<sup>2</sup> Department of Electronics and Computer Engineering, Hanyang University, Seoul, South Korea. <sup>3</sup> Department of Biomedical Engineering, Kwangju Women's University, South Korea.

The neutralization line technique provides good isolation between USB dongle antennas [34, 35]. Ultra-wideband MIMO antenna for USB dongle has been proposed with different patterns and polarizations in [36]. Furthermore, electromagnetic band-gap (EBG) structures [37, 38] and the use of lumped circuit decoupling networks [39, 40] are promising isolation techniques for MIMO antennas. In short, numerous choices of decoupling structures are available to antenna engineers for the design of MIMO antennas. However, selection of effective decouplers plays a significant role in the MIMO antenna performance, such as antenna bandwidth and efficiency.

Mobile device antennas are electrically small in size, which act as excitation elements for the ground plane of a mobile device. The antennas excite various characteristic current modes on the ground plane where the radiation performance mainly depends on the dominant ground mode. Installation of a decoupler on the ground plane of a mobile device for MIMO operation also affects the excited ground modes. The coupling between the ground mode and the decoupler depends on the (electric or magnetic) type of decoupler, which in turn affects the radiation and diversity performances of the MIMO antenna. In this investigation, a PIFA based MIMO antenna for a USB dongle has been analyzed when a T-type and loop-type decouplers are employed. The findings of the study can be applied to other mobile antennas for USB dongles as well; therefore, the choice of PIFA is arbitrary. The decouplers have been selected for this study because of their different nature of coupling with the fundamental ground mode. The T-type structure at the proposed location electrically couples with the ground mode whereas the loop-type structures couples magnetically with the ground mode. The analysis is based on the coupling mechanisms among the antenna, decoupler and dominant ground mode. The impacts of the decouplers on the performances of the MIMO antennas have been demonstrated using simulation and measured results. We emphasize that the decoupler must be carefully selected, considering its coupling with the dominant ground mode for high performance MIMO antenna design.

## 2. COUPLING MECHANISM AND MODAL ANALYSIS

The radiation performance of the PIFA depends on its coupling with the dominant ground mode. The PIFA acts as an electric coupler and its coupling ( $\alpha_e$ ) with the ground mode can be expressed as [41]

$$\alpha_e = \frac{1}{1 + \lambda} \iiint E^i \cdot J^g d\tau \quad (1)$$

where  $E^i$  is the impressed electric field produced by the antenna,  $J^g$  the dominant characteristic current mode of the ground plane, and  $\lambda$  the eigenvalue of the ground mode.  $E^i$  is strongest at the edge of the ground plane; therefore, placing the antenna at the location results in a stronger coupling with the ground mode. In the case of  $2 \times 2$  MIMO system, when PIFAs are installed at the edges of the ground plane, the antennas couple with the same ground mode, resulting in a strong mutual coupling. A parasitic resonator can be employed as a decoupler; however, depending on its type and location on the ground plane, it may affect the coupling between the antenna and the ground mode. In this study, the impact of decoupler on the MIMO antenna has been investigated for a USB dongle with a ground size  $60 \text{ mm} \times 30 \text{ mm}$ . The upper corners of the ground plane have been selected for the location of PIFA antennas for maximum coupling with the dominant ground mode. The middle of the longer edge of the ground plane has been selected for the location of T-type and loop-type decouplers.

In order to understand the coupling mechanism, the modal analysis of the ground plane is imperative. Figures 1 and 2 show the current distribution of the first two significant modes, mode 1 and mode 2, of the ground plane, respectively. Mode 1 resembles that of a half wave dipole that does not change phase across the ground plane. On the other hand, Mode 2 resembles that of a full wave dipole mode [42]. On the contrary to Mode 1, the current density of mode 2 is minimum at the middle of the longer edge of the ground plane. A particular mode radiates efficiently at resonance where the resonance frequency can be found when the eigenvalue of the mode is zero [43]. Figure 3 shows the eigenvalue plot of the modes, which reveals that mode 1 and mode 2 are resonant at 2.2 GHz and 5.5 GHz, respectively.

The T-type decoupler electrically couples with the dominant ground mode. According to Eq. (1), the coupling between the T-type decoupler and the first order mode will be minimum, because of minimum electric field of the ground mode at the middle of the ground plane. However, with second

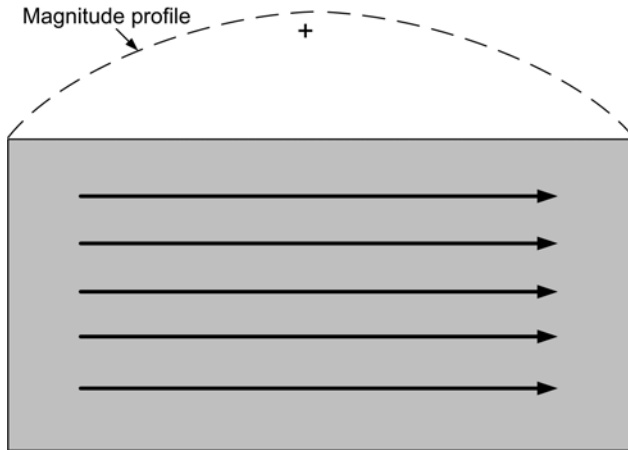


**Figure 1.** Current distributions of the ground mode 1.

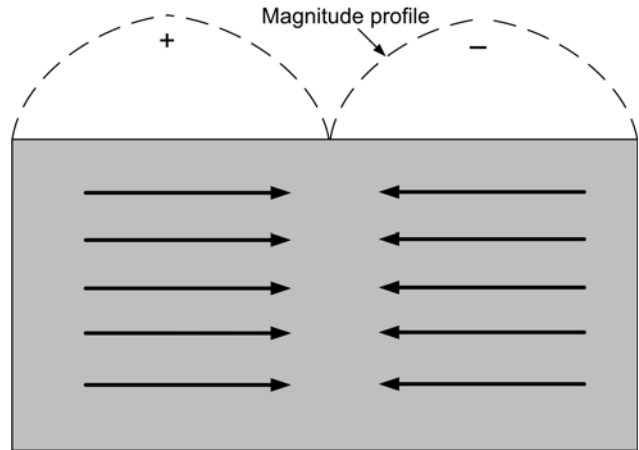


**Figure 2.** Current distributions of the ground mode 2.

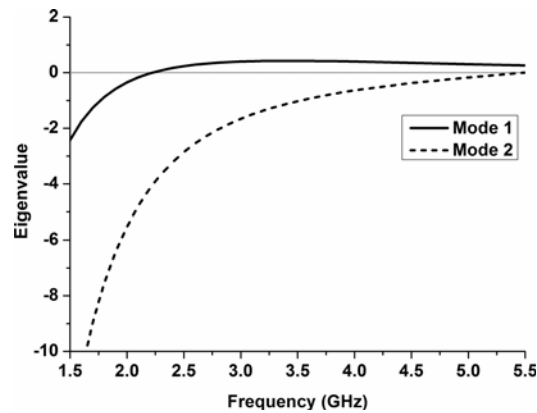


**Figure 3.** Eigenvalues of significant modes of the ground plane.

order mode, the coupling will be maximum. On the other hand, the loop-type decoupler magnetically couples with the dominant ground mode. The coupling between a magnetic coupler and the ground mode can be expressed as

$$\alpha_m = -\frac{1}{1 + \lambda} \iiint M^{loop} \cdot H^g d\tau \quad (2)$$

where  $M^{loop}$  is the magnetic current density of the loop, and  $H^g$  is the magnetic field of the ground mode. The coupling is strong when a magnetic coupler is located at the maximum magnetic field, i.e., the maximum current location of the ground mode. The strong coupling between the decoupler and the ground mode may degrade the coupling between the antennas and the ground mode, which could result in lower bandwidth and radiation efficiency of the MIMO antenna. The concept has been investigated in the following sections. The reduction of mutual coupling between the antennas does not depend on the modal analysis but depends on the choice of decoupler and its location on the ground plane. The characteristic mode analysis has been carried out to emphasize that the choice of the decoupler affects the coupling between the antenna and the ground mode that decides the radiation performance of the MIMO antenna.

### 3. MIMO ANTENNA DESIGN

The geometry of the reference antenna without the decoupling network is shown in Figure 4. The design consists of two symmetric PIFAs located at the corners of the longer edge of the ground plane. FR-4

( $\epsilon_r = 4.4$ ) has been used as a substrate material with 1.6 mm thickness. The size of the ground clearance for each antenna is 22 mm  $\times$  5 mm. Each PIFA consists of a single loop-feed structure and an antenna element. The length of the antenna element is 21 mm, and the size of the feed loop is 2 mm  $\times$  1 mm. In order to maintain the compact features, the antenna elements have been folded. The feed loop contains a series LC network to control the impedance level of the antenna [44]. Figure 5 shows the simulated current density when antenna 1 is excited and the other antenna terminated by the matched load. It can be observed that the antenna excites the current in the horizontal direction on the ground plane, i.e., the antenna is dominantly coupled with the first order mode. The antenna has been designed to operate at 2.45 GHz, where the simulated values of  $C_f$  and  $L_f$  are 2 pF and 2.5 nH, respectively. Both antennas are well matched at the design frequency where the simulated and measured bandwidths (with reference to  $-10$  dB) are 100 MHz and 140 MHz, respectively. The simulated radiation efficiency is 73.26% at the operating frequency. The antenna has been fabricated where the fabricated  $C_f$  and  $L_f$  values are 1.5 pF and 2 nH, respectively. The results have been measured using an Agilent 8753ES network analyzer. In order to improve the isolation, a decoupler needs to be employed. The effects of T-type and loop-type decouplers on the bandwidth of MIMO antenna are discussed in the following subsections.

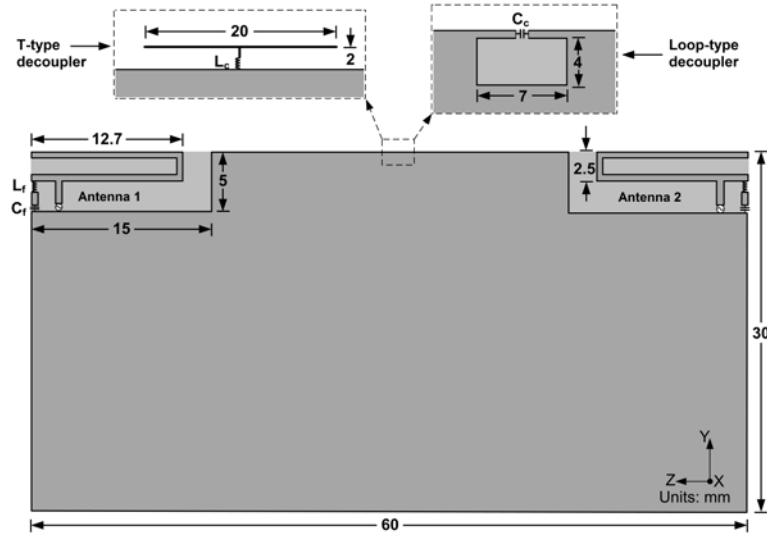


**Figure 4.** Geometry of the decouplers and MIMO antenna.

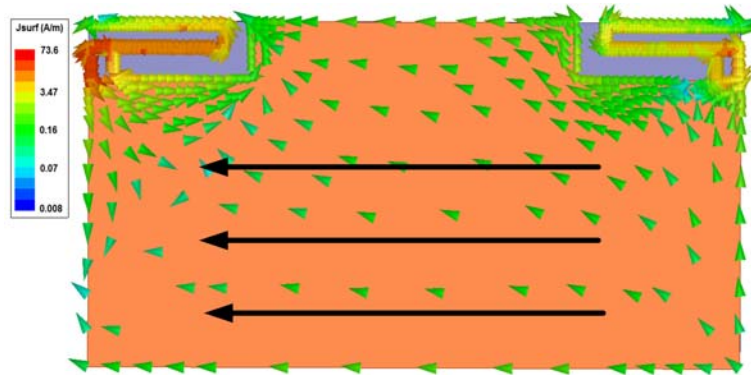


**Figure 5.** Simulated current density at 2.45 GHz.

### 3.1. Effect of the T-Type Decoupler

The T-type decoupler consists of a 20 mm wire and is connected with the ground plane through a 2 mm wire and an inductor  $L_c$ . The decoupler has been installed between the PIFA antennas, as indicated

in Figure 4. The inductor  $L_c$  has been employed to maintain the compact features of the decoupler such that it can be easily accommodated in the rim of a USB dongle [45]. The frequency of a coupling null can be controlled using  $L_c$  where increasing the value of  $L_c$  decreases the frequency of the coupling null. The simulated and measured  $s$ -parameters are displayed in Figure 6. The simulated and measured matching bandwidths are 240 MHz and 290 MHz, respectively. The simulated radiation efficiency of the antenna is 87.79%. The minimum value of the measured  $S_{12}$  is  $-34.01$  dB when the fabricated  $L_c$  is 4.7 nH, due to the strong coupling between the antenna and decoupler. The measured  $S_{12}$  of the reference antenna is also displayed in Figure 6 for comparison. At the design frequency, the  $S_{12}$  of the reference antenna is  $-10.7$  dB. The simulated current density of the MIMO system, when antenna 1 is excited and antenna 2 terminated by the matched load, is shown in Figure 7. It can be observed that the current is strongly coupled with the T-type decoupler. Along with the direct path, the current of antenna 1 takes an additional path through the decoupler, creating a current null at the port of antenna 2. The comparison of the current densities of Figure 5 and Figure 7 shows that the decoupler does not significantly affect the current density of the ground plane, indicating that the coupling between the decoupler and the first order ground mode is very weak. The observations are in agreement with the proposed theory of Section 2.

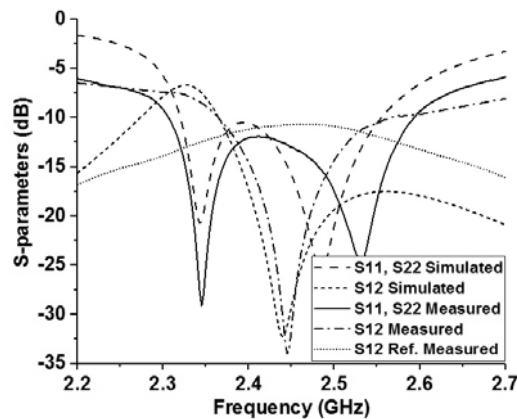


Figure 6. Simulated and measured  $S$ -parameters with the T-type decoupler.

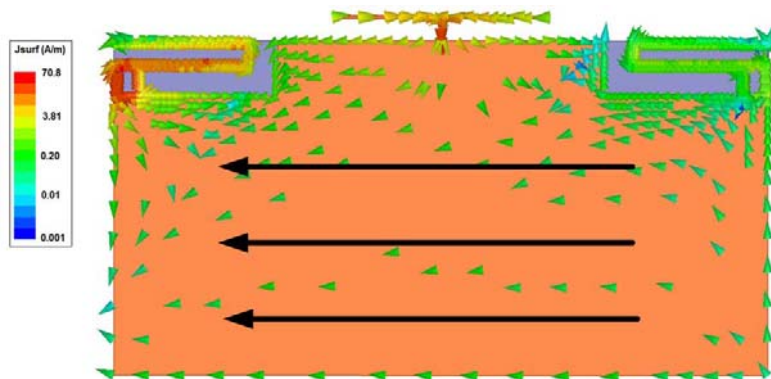
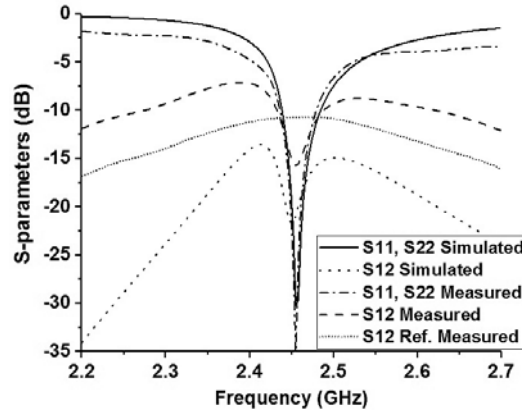


Figure 7. Simulated current density at 2.45 GHz.

### 3.2. Effect of the Loop-Type Decoupler

The loop-type decoupler is employed between the antennas by etching a ground clearance  $7\text{ mm} \times 4\text{ mm}$  in size, as shown in Figure 1. Capacitor  $C_c$  is used to control the resonance frequency of the decoupler where increasing the value of  $C_c$  tunes the decoupling null to lower frequency. The simulated and measured  $S$ -parameters are presented in Figure 8. In this case, both the simulated and measured



**Figure 8.** Simulated and measured  $S$ -parameters with the loop-type decoupler.

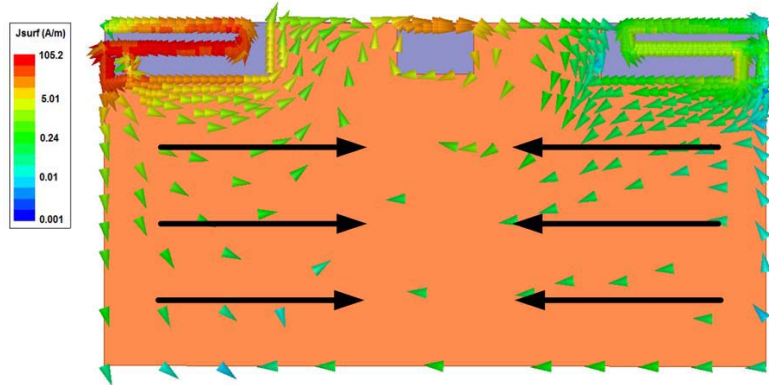


**Figure 9.** Simulated current density at 2.45 GHz.

matching bandwidths are 40 MHz, whereas the simulated radiation efficiency of the antenna at the design frequency is 78.35%. Moreover, the measured  $S_{12}$  is  $-15.72$  dB at the design frequency when  $C_c$  is 0.4 pF, indicating weaker coupling between the antenna and decoupler. The bandwidth, isolation and efficiency of the antenna in this case are significantly less than that of the T-type decoupler. The simulated current density of the MIMO antenna with loop-type decoupler is presented in Figure 9. The comparison of Figure 9 and Figure 5 shows that the decoupler significantly affects the current density of the ground plane indicating stronger coupling between the ground mode and the decoupler. The excited currents on the ground plane reveal that the coupling of the antennas with second order mode is more dominant than the first order mode. As shown in Figure 3, the eigenvalue of mode 2 is more reactive (capacitive) than the first order mode at the operating frequency that results in poor coupling between the antenna and the ground modes. Therefore, the loop-type decoupler resulted in poor bandwidth performance of the MIMO antenna.

#### 4. COMPARISON OF RADIATION PERFORMANCE

In order to compare the radiation and diversity performances of the MIMO antennas, the results are measured in a  $6\text{ m} \times 3\text{ m} \times 3\text{ m}$  3D CTIA OTA anechoic chamber. The envelop correlation coefficients (ECC)  $\rho_e$  of the antennas were measured using the expression

$$\rho_e = \frac{\left| \iint_{4\pi} F_1(\theta, \phi) F_2(\theta, \phi) d\Omega \right|^2}{\iint_{4\pi} |F_1(\theta, \phi)|^2 d\Omega \iint_{4\pi} |F_2(\theta, \phi)|^2 d\Omega} \quad (3)$$

where  $F_i(\theta, \phi)$  is the radiation pattern of the MIMO antenna when port  $i$  is excited [46]. The value of ECC for the mobiledevice MIMO antennas should be less than 0.5. The ECC and total radiation efficiency of the MIMO antennas are presented in Figures 10 and 11, respectively. As shown in Figure 10, the ECCs with both decouplers satisfy the 0.5 criterion. The ECCs with the T-type and loop-type decouplers in the operating frequency are 0.05 and 0.17, respectively. Figure 11 shows that the radiation efficiency with the T-type decoupler is significantly higher than the case of loop-type decoupler. The measured total radiation efficiencies of the MIMO antenna with the T-type decoupler, loop-type decoupler and reference antenna are 50.62%, 38.71% and 44.08%, respectively.

The measured radiation patterns of the MIMO antennas at 2.45 GHz are presented in Figures 12, 13 and 14. The patterns have been measured by exciting one antenna and terminating the other antenna by a matched load. The comparison of Figures 13 and 14 with Figure 12 shows that the decouplers influence the co- and cross-polarizations in the  $YZ$  plane differently; however, the co- and cross-polarizations in  $XZ$  and  $XY$  planes have not been affected significantly. The measured peak gains of the reference antenna, MIMO with T-type decoupler and MIMO with loop-type decoupler are  $-0.45$  dBi,  $-0.04$  dBi and  $-0.65$  dBi, respectively. The data indicate that the radiation and diversity performances of the MIMO antenna with the T-type decoupler are better than that of loop-type decoupler.

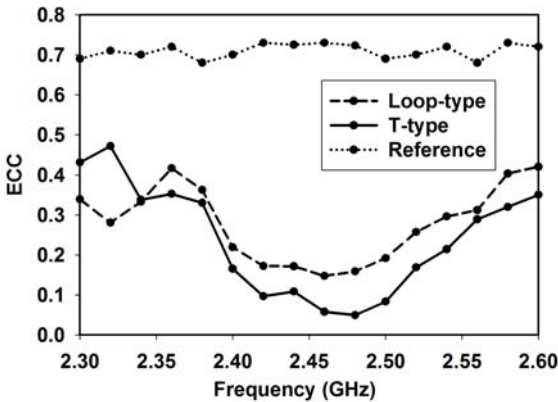


Figure 10. The measured ECC of the MIMO antennas.

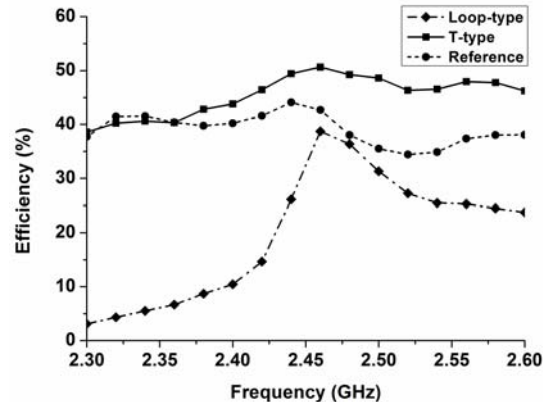


Figure 11. The measured total efficiency of the MIMO antennas.

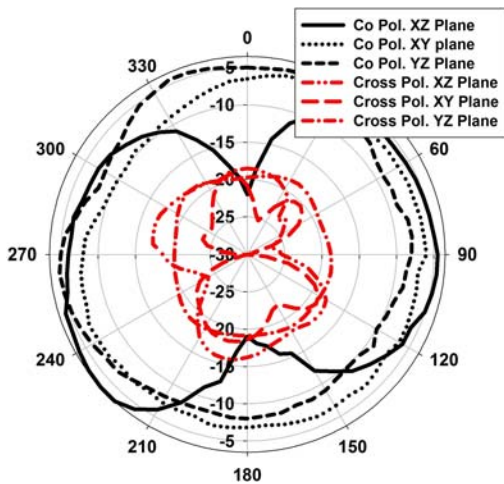


Figure 12. The measured radiation patterns of the reference antenna.

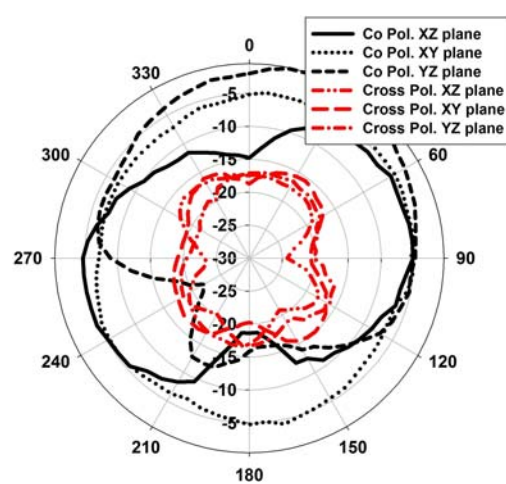
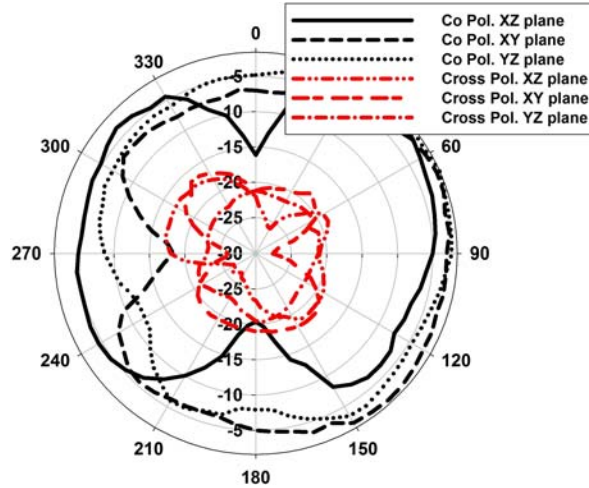


Figure 13. The measured radiation patterns of MIMO antenna with T-type decoupler.



**Figure 14.** The measured radiation patterns of MIMO antenna with loop-type decoupler.

## 5. CONCLUSION

In this paper, the radiation and diversity performances of PIFA-based MIMO antennas were analyzed based on the coupling between the decoupler and the ground mode. It was observed that the excitation of the dominant mode on the ground plane depends on the choice of decoupler that in turn affects the radiation efficiency. Strong coupling between the antenna and the decoupler resulted in good diversity performance; however, strong coupling between the dominant ground mode and the decoupler affected the coupling between the ground mode and the antenna, resulting in poor radiation performance. Therefore, in the design of high performance MIMO antennas for mobile devices, the decoupler must be judiciously selected considering its coupling with the dominant ground mode.

## ACKNOWLEDGMENT

This work was supported by the ICT R & D program of the MSIP/IITP, Republic of Korea (2013-0-00401, Ground radiation technique for mobile devices).

## REFERENCES

1. Foschini, Jr., G. J., "Layered spacetime architecture for wireless communication in a fading environment when using multi-element antennas," *Bell Labs Tech. J.*, Vol. 1, No. 2, 41–59, 1996.
2. Foschini, Jr., G. J. and M. J. Gans, "On limits of wireless communication in a fading environment when using multiple antennas," *Wireless Personal Commun.*, Vol. 6, 311–335, 1998.
3. Jeon, S., Y. Liu, S. Ju, et al., "PIFA with a parallel resonance feed structure for wide-band operation," *Electronics Letters*, Vol. 47, No. 23, 1263–1265, 2011.
4. Lee, J., Y. Liu, H. Kim, et al., "PIFA with a dual resonance feed structure for enhancement of impedance bandwidth," *Electronics Letters*, Vol. 49, No. 15, 921–922, 2013.
5. Liu, Y., X. Lu, H. Jang, et al., "Loop-type ground antenna using resonated loop feeding, intended for mobile devices," *Electronics Letters*, Vol. 49, No. 7, 426–427, 2013.
6. Liu, Y., J. Lee, H. Kim, et al., "Ground radiation method using slot with coupling capacitors," *Electronics Letters*, Vol. 49, No. 15, 921–922, 2013.
7. Elghannai, E. A. and R. G. Rojas, "Design of USB dongle antenna for WLAN applications using theory of characteristic modes," *Electronics Letters*, Vol. 50, No. 4, 249–251, 2014.
8. Liu, W.-C. and Y.-L. Chen, "Compact strip-monopole antenna for WLAN-band USB dongle application," *Electronics Letters*, Vol. 47, No. 8, 479–480, 2011.

9. Liao, W.-J., S.-H. Chang, J. T. Yeh, et al., "Compact dual-band WLAN diversity antennas on USB Dongle platform," *IEEE Trans. Antennas Propag.*, Vol. 62, No. 1, 109–118, 2014.
10. Lee, C.-J., L.-T. Hwang, T. S. Horng, et al., "A MIMO antenna with built-in isolation for WLAN USB dongle applications," *Asia-Pacific Microwave Conference, Proceedings*, 1055–1057, 2013.
11. Tseng, Y.-K., Y.-C. Lin, L. T. Hwang, et al., "Implementation of a MIMO antenna design for USB dongle applications," *Electronic Components and Technology Conference*, 2089–2094, 2013.
12. Li, Z., Z. Du, M. Takahashi, et al., "Reducing mutual coupling of MIMO antennas with parasitic elements for mobile terminals," *IEEE Trans. Antennas Propag.*, Vol. 60, No. 2, 473–481, 2012.
13. Wu, T. Y., S. T. Fang, and K. L. Wong, "Printed diversity monopole antenna for WLAN operation," *Electronics Letters*, Vol. 38, No. 25, 1625–1626, 2002.
14. Toktas, A. and A. Akdagli, "Wideband MIMO antenna with enhanced isolation for LTE, WiMAX and WLAN mobile handsets," *Electronics Letters*, Vol. 50, No. 10, 723–724, 2014.
15. Chi, G., L. Binhong, and D. Qi, "Dual-band printed diversity antenna for 2.4/5.2 GHz WLAN application," *Microw. Opt. Technol. Lett.*, Vol. 45, No. 6, 561–563, 2005.
16. Choukiker, Y. K., S. K. Sharma, and S. K. Behera, "Hybrid fractal shape planar monopole antenna covering multiband wireless communications with MIMO implementation for handheld mobile devices," *IEEE Trans. Antennas Propag.*, Vol. 62, No. 3, 1483–1488, 2014.
17. Yao, Y., X. Wang, X. Chen, et al., "Novel diversity/MIMO PIFA antenna with broadband circular polarization for multimode satellite navigation," *IEEE Antennas and Wireless Propag. Letters*, Vol. 11, 65–68, 2012.
18. Khan M. S., A. D. Capobianco, A. I. Najam, et al., "Compact ultra-wideband diversity antenna with a floating parasitic digitated decoupling structure," *IET Microw. Antennas Propag.*, Vol. 8, No. 10, 747–753, 2014.
19. Li, J. F., A. X. Chu, and T. G. Huang, "A compact wideband MIMO antenna with two novel bent slits," *IEEE Trans. Antennas Propag.*, Vol. 60, No. 2, 482–489, 2012.
20. Kokkinos, T., E. Liakou, and A. P. Feresidis, "Decoupling antenna elements of PIFA arrays on handheld devices," *Electronics Letters*, Vol. 44, No. 25, 1442–1444, 2008.
21. Zhang, S., B. K. Lau, Y. Tan, et al., "Mutual coupling reduction of two PIFAs with a T-shape slot impedance transformer for MIMO mobile terminals," *IEEE Trans. Antennas Propag.*, Vol. 60, No. 3, 1521–1531, 2012.
22. Saraereh, O. A., C. J. Panagamuwa, and J. C. Vardaxoglou, "Low correlation multiple antenna system for mobile phone applications using novel decoupling slots in ground plane," *IEEE Antennas and Propagation Conf.*, 577–581, Loughborough, England, 2013.
23. Qu, L., R. Zhang, and H. Kim, "Decoupling between ground radiation antennas with ground-coupled loop-type isolator for WLAN applications," *IET Microw. Antennas Propag.*, Vol. 10, No. 5, 546–552, 2016.
24. Qu, L., H. Lee, H. Shin, et al., "MIMO antennas using controlled orthogonal characteristic modes by metal rims," *IET Microw. Antennas Propag.*, Vol. 11, No. 7, 1009–1015, 2017.
25. Szini, I., A. Tatomirescu, and G. F. Pedersen, "On small terminal MIMO antennas, harmonizing characteristic modes with ground plane geometry," *IEEE Trans. Antennas Propag.*, Vol. 63, No. 4, 1487–1497, 2015.
26. Kishor, K. and V. A. Hum, "Two-port chassis-mode MIMO antenna," *IEEE Trans. Antennas Propag.*, Vol. 62, No. 6, 3290–3298, 2014.
27. Kishor, K. and V. A. Hum, "Multiport multiband chassis-mode antenna design using characteristic modes," *IEEE Antennas and Wireless Propag. Letters*, Vol. 16, 609–612, 2017.
28. Qin, P., Y. J. Guo, R. Andrew, et al., "A pattern reconfigurable U-slot antenna and its applications in MIMO systems," *IEEE Trans. Antennas Propag.*, Vol. 60, No. 2, 516–528, 2012.
29. Ren, J., X. Yang, J. Yin, and Y. Yin, "A novel antenna with reconfigurable patterns using H-shaped structures," *IEEE Antennas and Wireless Propag. Letters*, Vol. 14, 915–918, 2015.
30. Rhee, C., Y. Kim, T. Park, et al., "Pattern-reconfigurable MIMO antenna for high isolation and low correlation," *IEEE Antennas and Wireless Propag. Letters*, Vol. 13, 1373–1376, 2014.

31. Zhou, Y., S. Raviraj, and S. V. Hum, "Design and evaluation of pattern reconfigurable antennas for MIMO applications," *IEEE Trans. Antennas Propag.*, Vol. 62, No. 3, 1084–1092, 2014.
32. Malviya, L., R. K. Panigrahi, and M. V. Kartikeyan, "A  $2 \times 2$  dual-band MIMO antenna with polarization diversity for wireless applications," *Progress In Electromagnetics Research C*, Vol. 61, 91–103, 2016.
33. Sharawi, M. S., M. Ikram, and A. Shamim, "A two concentric slot loop based connected array MIMO antenna system for 4G/5G terminals," *IEEE Trans. Antennas Propag.*, Vol. 65, No. 12, 6679–6686, 2017.
34. Su, S. W., C. T. Lee, and F. S. Chang, "Printed MIMO-antenna system using neutralization-line technique for wireless USB-dongle applications," *IEEE Trans. Antennas Propag.*, Vol. 60, No. 9, 456–463, 2012.
35. Li, Z., M. S. Han, X. Zhao, et al., "MIMO antenna with isolation enhancement for wireless USB dongle application at WLAN band," *Proc. Asia-Pacific Microw. Conf. (APMC)*, 758–761, 2010.
36. Zhang, S., B. K. Lau, Sunesson, et al., "Closely-packed UWB MIMO/diversity antenna with different patterns and polarizations for USB dongle applications," *IEEE Trans. Antennas Propag.*, Vol. 60, No. 9, 4372–4380, Sep. 2012.
37. Lei, Q., F. Zhao, K. Xiao, et al., "Transmit receive isolation improvement of antenna arrays by using EBG structures," *IEEE Antennas and Wireless Propag. Letters*, Vol. 11, 93–96, 2012.
38. Yang, F. and Y. Samii, "Microstrip antennas integrated with electromagnetic band gap structures: A low mutual coupling design for array applications," *IEEE Trans. Antennas and Propag.*, Vol. 51, No. 10, 2936–2946, 2003.
39. Tang, X., K. Mouthaan, and J. C. Coetzee, "Tunable decoupling and matching network for diversity enhancement of closely spaced antennas," *IEEE Antennas and Wireless Propag. Letters*, Vol. 11, 268–271, 2012.
40. Chen, S. C., Y. S. Wang, and S. J. Chung, "A decoupling technique for increasing the port isolation between two strongly coupled antennas," *IEEE Trans. Antennas Propag.*, Vol. 56, No. 12, 3650–3658, 2008.
41. Harrington, R. F., *Time-Harmonic Electromagnetic Fields*, Macgraw-Hill, New York, 1961.
42. Zahid, Z. and H. Kim, "Tunable slot type ground radiation antenna with dual band operation using LC resonator," *Journal of Electromagnetic Engineering and Science*, Vol. 17, No. 2, 71–75, 2017.
43. Cabedo, M., E. Antonino, A. Valero, et al., "Theory of characteristic modes revisited: A contribution to the design of the antennas for modern applications," *IEEE Trans. Antennas and Propagation Magazine*, Vol. 49, No. 5, 52–68, 2007.
44. Lee, J., Y. Liu, and H. Kim, "Mobile antenna using multi-resonance feed structure for wideband operation," *IEEE Trans. Antennas Propag.*, Vol. 62, No. 11, 5851–5855, 2014.
45. Qu, L., R. Zhang, H. Shin, et al., "Performance enhancement of ground radiation antenna for Z-wave applications using tunable metal loads," *Electronics Letters*, Vol. 52, No. 22, 1827–1828, 2016.
46. Vaughan, R. G. and J. B. Andersen, "Antenna diversity in mobile communications," *IEEE Trans. Veh. Technol.*, Vol. 36, No. 4, 149–172, 1987.